Electrochimica Acta 272 (2018) 161–168

Contents lists available at ScienceDirect

Electrochimica Acta

journal homepage: www.elsevier.com/locate/electacta

$NiCoSe_{2-x}$/N-doped C mushroom-like core/shell nanorods on N-doped carbon fiber for efficiently electrocatalyzed overall water splitting

Jiang Li [b], Meng Wan [b], Tao Li [b], Han Zhu [a, b], Zhenghuan Zhao [c], Zheng Wang [c], Weiwei Wu [c, **], Mingliang Du [a, b, *]

[a] Key Laboratory of Synthetic and Biological Colloids, Ministry of Education, School of Chemical and Material Engineering, Jiangnan University, Wuxi, 214122, PR China
[b] College of Materials and Textiles, Zhejiang Sci-Tech University, Hangzhou, 310018, PR China
[c] School of Advanced Materials and Nanotechnology, Xidian University, Shaanxi, 710126, PR China

ARTICLE INFO

Article history:
Received 19 September 2017
Received in revised form
2 February 2018
Accepted 4 April 2018
Available online 5 April 2018

Keywords:
N-doped carbon
Nickel-cobalt diselenide
Core/shell nanorod
Selenization
Overall water splitting

ABSTRACT

Developing stable and efficient bifunctional catalysts for overall water splitting is a critical step in the production of renewable energy sources. Here we report a stable and highly active electrocatalyst comprised of $NiCoSe_{2-x}$/N-doped carbon mushroom-like core/shell nanorods on silk-derived carbon fiber through one step selenization. The unique one-dimensional nanorod structure facilitates the charge transport, and the N-doped carbon shell also increases the electrical conductivity, resulting in a remarkable enhancement of the catalytic activity. The N-doped carbon shell also functions as a protection layer. The composite catalyst therefore exhibits outstanding OER and HER performance, it can also stably drive the overall water splitting at a low cell voltage of 1.53 V in base solution. The present work provides an efficient strategy for the fabrication of stable and active electrocatalysts with earth-abundant elements.

1. Introduction

The development of clean and renewable energy sources holds the promise for the solution of environmental contamination and energy crisis [1–3]. Hydrogen has been recognized as the center of newly emerged hydrogen economy, and water electrolysis is the most efficient way for the clean and sustainable production of hydrogen when coupled with renewable solar and wind [4–7]. Water electrocatalysis is an uphill process and consisted of two half reactions including the hydrogen evolution reaction (HER) and the oxygen evolution reaction (OER), with the latter more challenging [8,9]. Up to date, the best electrocatalysts for the HER and the OER are noble Pt and Ir-based compounds, respectively [10,11]. However, the high cost of noble metals limits their industrial applications. It is important to develop active electrocatalysts using earth-abundant elements [12,13].

Much effort has been made for the development of transition metal-based electrocatalysts [14–16]. Of a particularly, Ni and Co based nanomaterials show outstanding catalytic activity toward HER, OER and even overall water electrolysis [17–19]. Recently, transition metal selenides (TMSs) have been demonstrated to be very active electrocatalysts in HER and OER. However, many TMSs are unavoidable to be oxidized in base electrolyte, or corroded in acidic media, and hence serve as the precatalyst for the catalytic reaction [20]. In addition, the vast majority of existing TMSs are unsuitable for use in the same electrolyte because of the mismatch of pH ranges in which the electrocatalysts are both stable and sufficiently active. It is therefore important to develop new strategies to fabricate these high-performance materials.

Most recently, nickel cobalt diselenide has been reported to be active for HER [21,22], but with few report on OER probably because of the stability issue. It has been shown that carbon-based materials can not only increase the catalysts stability but also contributed to the catalytic reaction [23–26].

In this work, to solve the mentioned concerns on the catalyst stability and further improve the performance, we developed a facile on-step selenization method to synthesize a core/shell nanorod structure with the nickel-cobalt diselenide nanorod core

* Corresponding author. Key Laboratory of Synthetic and Biological Colloids, Ministry of Education, School of Chemical and Material Engineering, Jiangnan University, Wuxi, 214122, PR China.
** Corresponding author.
E-mail addresses: wwwu@xidian.edu.cn (W. Wu), du@jiangnan.edu.cn (M. Du).

https://doi.org/10.1016/j.electacta.2018.04.032
0013-4686/

protected by N-doped carbon shell on silk-derived carbon fiber. The core/shell nanorod on carbon fiber can directly be employed as the binder-free electrode to drive overall water splitting, with the cell voltage as low as 1.53 V at 10 mA cm^{-2}. The present work demonstrates an efficient route for the development of robust bifunctional electrochemical catalysts of water splitting.

2. Experimental methods

2.1. Chemicals and materials

Acetone, alcohol, deionized water and N,N-Dimethylformamide were purchased from Hangzhou Gaojing Fine Chemical Industry Co., Ltd. (Zhejiang China). Cobalt nitrate hexahydrate ($Co(NO_3)_2 \cdot 6H_2O$), Nickle nitrate hexahydrate ($Ni(NO_3)_2 \cdot 6H_2O$) and selenium powder were purchased from Shanghai Macklin Biochemical Co., Ltd. (Shanghai China).

2.2. Preparation of the $NiCoSe_{2-x}$/NC precursor

Silk was cleaned in acetone, alcohol, deionized water by ultrasonication and dried in vacuum at 60 °C overnight. Then, 1 g of clean silk was immersed in a deep-red solution containing 1.16 g of $Ni(NO_3)_2$, 1.16 g of $Co(NO_3)_2$ and N,N-dimethylformamide. After 24 h, the silk was picked up and dried at 60 °C overnight. The above immersing-drying process was repeated to ensure enough metal salts are loaded onto the silk.

2.3. Synthesis of $NiCoSe_{2-x}$/NC nanomushroom arrays grown on the silk-derived carbon fibers

The selenization process was conducted in a tube furnace. An alumina boat loaded with the silk and precursor was placed in the center of a quartz tube, and another alumina boat loaded with 0.3 g of Se powder was placed at the upstream side in the tube with the distance of 26 cm from the silk boat. The silk boat was heated to 230 °C from room temperature at the rate of 5 °C/min and maintained for 3 h at 230 °C in air. Then Ar gas (150 sccm) was introduced and the temperature was ramped to 900 °C and kept for 3 h. For comparison, Ni_3Se_4 and CoSe were prepared with the same method.

2.4. Electrochemical measurements

Electrochemical measurements were carried out using an electrochemical work station (Ivium A88441). All of the measurements were performed using a three-electrode cell with an Ag/AgCl electrode as the reference. A platinum net and a graphite rod were used as the counter electrode in OER and HER tests, respectively. The samples were cut into regular flakes (0.9 cm × 0.6 cm) and the mass is 5.76 mg. The total loading of $NiCoSe_{2-x}$ is about 4.54 mg calculated according to the SEM-EDS results. The samples were directly used as the binder-free working electrode and 0.5 M H_2SO_4 and 1.0 M KOH were used as the electrolytes. Linear sweep voltammetry (LSV) was performed at scan rate of 0.2 mV/s to obtain the polarization curves. Cyclic voltammetry (CV) was carried out from −0.244 V to 0.556 V with the scan rate of 0.5 mV/s. Electrochemical impedance spectroscopy (EIS) was employed when the working electrode was biased at a constantly value of −0.23 V *vs.* reversible hydrogen electrode (RHE) while sweeping the frequency from 5 MHz to 10 MHz.

2.5. Characterizations

The structures of the synthesized samples were characterized by field emission scanning electron microscopy (FE-SEM) under the accelerating voltage of 3 kV (ULTRA55, ZEISS, Germany). Transmission electron microscopy (TEM) was carried out on a JSM-2100 (JEOL, Japan) and the high-angle annular dark field scanning transmission electron microscopy (HAADF-STEM) images as well as the line-scan energy dispersive X-ray spectroscopy (EDX) were conducted on a STEM (Tecnai G2 F30 S-Twin, Philips-FEI) at the accelerating voltage of 300 kV. X-ray diffraction (XRD) patterns were recorded on Bruker Axs D8 Discovery instrument with a Cu Kα line. The chemical state of elements was analyzed on X-ray photoelectron spectrometer (XPS, Kratos Axis Ultra DLD) under the Al Kα source (1486.6 eV).

3. Results and discussion

Fig. 1 shows the schematic illustration of the fabrication of $NiCoSe_{2-x}$/N-doped C (denoted as $NiCoSe_{2-x}$/NC) nanomushroom arrays on the silk-derived carbon fibers as advanced electrocatalysts for water splitting. The XRD patterns of $NiCoSe_{2-x}$/NC, CoSe and Ni_3Se_4 are revealed in Fig. 2a. The as-prepared $NiCoSe_{2-x}$/NC is indexed to hexagonal phase (PDF#65-7038), while the CoSe and Ni_3Se_4 belong to hexagonal and monoclinic phase, respectively. The broad peak at 24.2° marked by green triangle is assigned to the (002) plane of graphitized carbon. Raman analysis (Fig. 2b) was further confirmed the existence of graphitized carbon with obvious D and G peak located at 1331 and 1572 cm^{-1}, respectively [27]. It is clear that the peaks of $NiCoSe_{2-x}$/NC are not the simple superimposition of Ni_3Se_4 and CoSe, in addition, the intense bonds of $NiCoSe_{2-x}$/NC which located at the 459 cm^{-1} and 657 cm^{-1} have a smaller blue shift comparing to those of CoSe. The possible reason is that the Ni atom instead of Co atom causing the new chemical bond [22,28].

The morphology of the prepared samples was characterized by SEM as shown in Fig. 3. The $NiCoSe_{2-x}$/NC displays uniform nanorods with mushroom-like morphology vertical to the carbon support (Fig. 3a and d). The cross-section view image (Fig. S1) reveals that the length and the diameter of the nanorod are 0.535 μm and 0.105 μm, respectively. The SEM images of the Ni_3Se_4 (Fig. 3b and e) and CoSe (Fig. 3c and f) indicate the both the Ni_3Se_4 and CoSe show polyhedron morphologies and are homogeneously distributed on the silk-derived carbon fibers. The results of SEM-EDS elemental mapping indicate the existence of Ni, Co and Se with the ratio of about 1:1.19:1.55 for the $NiCoSe_{2-x}$/NC sample (Fig. S2 and Table 1).

The mushroom-like morphology of the vertical $NiCoSe_{2-x}$/NC nanorod was further confirmed by TEM characterization in Fig. 4a. The measured the length and the diameter of the nanorod is about 0.534 μm and 0.108 μm (Fig. S3), in good agreement with the SEM results. High resolution TEM images in Fig. 4b and c shows the nanorod has a core/shell structure. The thickness of the carbon shell is about 13.56 nm. The measured distance of the lattice fringe is 0.367 nm and 0.323 nm, corresponding to the (002) plane of graphitized carbon and the (100) plane of hexagonal $NiCoSe_{2-x}$. Besides, the lattice d-spacing in Fig. 4c and d is measured to be 0.216 nm and 0.285 nm, assigned to the (102) and (101) planes of the hexagonal phase $NiCoSe_{2-x}$, respectively. The selected-area electron diffraction (SAED) pattern image exhibits bright spots (Fig. 4e), suggesting the single crystallinity of the as-synthesized $NiCoSe_{2-x}$ rather than the mixed phase of CoSe and Ni_3Se_4. The patterns are assigned to the (100), (102) and (002) planes of hexagonal $NiCoSe_{2-x}$. The elemental composition was first analyzed by TEM-EDX elemental mapping of the selected area in Fig. 4a (green square). The results show the existence of Ni, Co and Se with the atomic ratio of about 1:1.01:1.63, as well as C and N (Fig. S4).

Scanning transmission electron microscopy (STEM) and EDX mapping were used to characterize the elements distribution

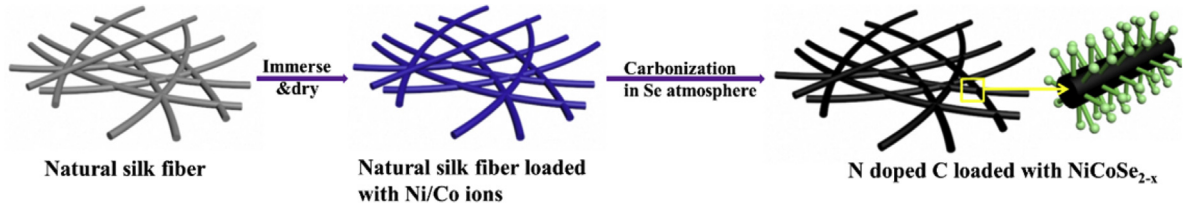

Fig. 1. Schematic illustration of the fabrication of $NiCoSe_{2-x}$/NC core/shell nanorod arrays on the silk-derived carbon fibers.

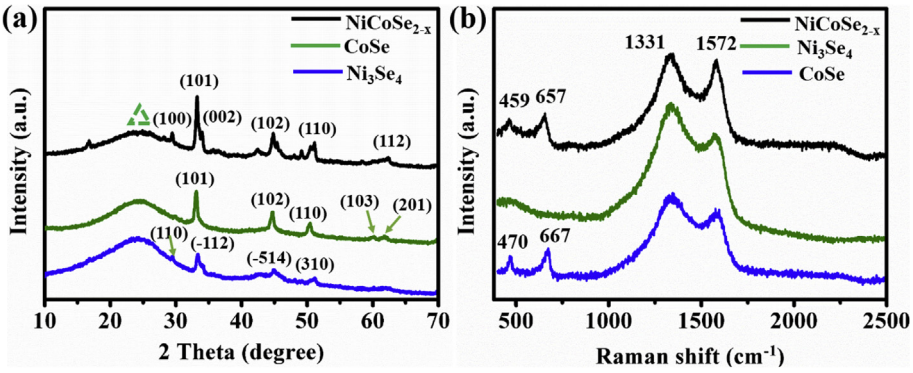

Fig. 2. (a) XRD and (b) Raman pattern of the $NiCoSe_{2-x}$/NC core/shell nanorod.

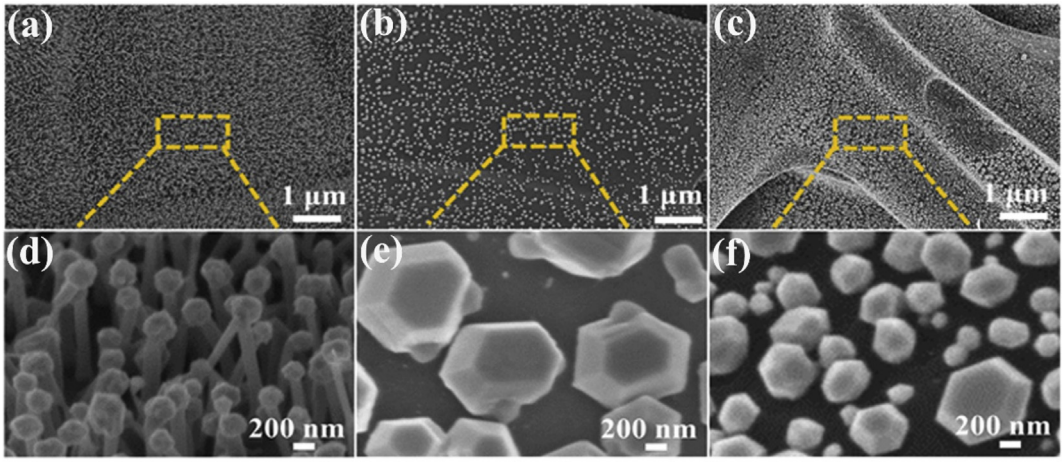

Fig. 3. (a–c) SEM images of the $NiCoSe_{2-x}$/NC core/shell nanorod, Ni_3Se_4 and CoSe at low-magnification as well as the high-magnification (d–f), respectively.

Table 1
The atomic ratio of three samples.

	C	N	O	Ni	Co	Se
Ni_3Se_4	84.54%	6.15%	4.25%	2.97%	–	2.09%
CoSe	75.96%	3.61%	7.20%	–	6.44%	6.79%
$NiCoSe_{2-x}$/NC	51.58%	2.16%	5.49%	10.89%	12.97%	16.91%

(Fig. 5). All the elements including C, N, Co, Ni and Se are homogeneously distributed across the whole nanorod. It is found that the distribution of C and N is wider than those of Ni, Co and Se (Fig. 5a), implying that N exists in the carbon shell of the composite. This result is further demonstrated by the results of line-scan EDX mapping of the top end (Fig. 5b) and the middle of the nanorod (Fig. 5c). The C and N signals appeared before the signal of Ni, Co and Se, and disappeared after the disappearance of the Ni, Co and Se signals (Fig. 5b and c).

The chemical state of $NiCoSe_{2-x}$/N-doped C@carbon fiber was characterized by X-ray photoelectron spectroscopy (XPS), as shown in Fig. 6. The XPS survey spectrum shows the existence of C, N, O, Ni, Co and Se (Fig. 6a). The Ni shows two spin-orbit doublets and two shake-up satellites (Fig. 6b) [29], and the Co displays two mains peaks at 780.2 eV and 796.2 eV, corresponding to the $2p_{3/2}$ and $2p_{1/2}$ (Fig. 6c) [30], respectively. These binding energies are indicative of metal selenides [21], confirmed by the Se $3d_{5/2}$ (54.4 eV) and $3d_{3/2}$ (55.3 eV) in Fig. 6d. The peak at 59.4 eV (Se $3d_{5/2}$) is probably ascribed to the surface oxide species Se-O bonds [28,31].

The electrochemical measurements for evaluating the activities of the present samples were conducted with a three-electrode configuration. We first investigated the OER activities in 1.0 M KOH. Fig. 7a shows the polarization curves after *IR* correction and corresponding Tafel slopes. The silk-derived carbon fibers (SCFs) possess a negligible OER activity with the onset potential at 1.90 V while 1.60 V and 1.57 V for Ni_3Se_4 and CoSe, respectively. The

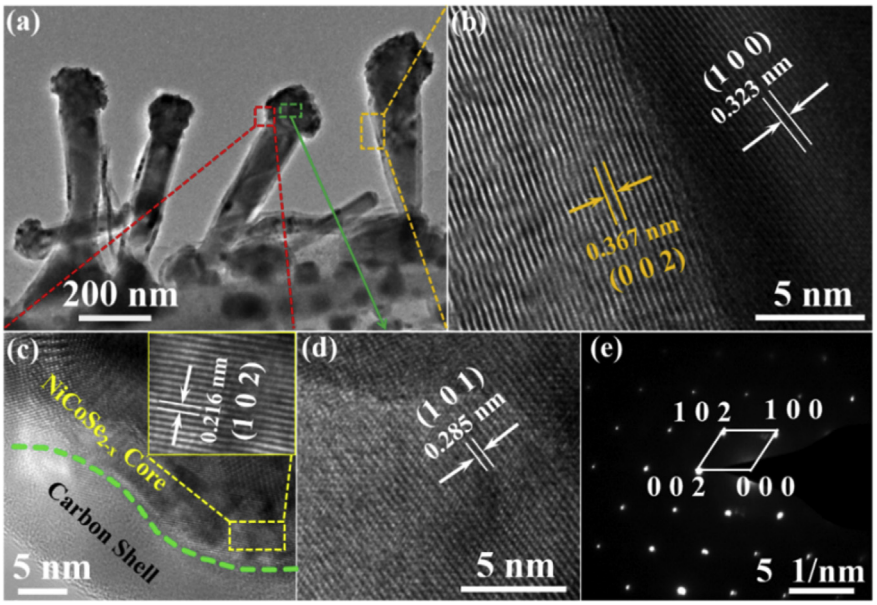

Fig. 4. (a) TEM image of the $NiCoSe_{2-x}$/NC core/shell nanorod arrays. (b–d) The HRTEM images about nanorod and nanoparticles selected from in Fig. 1. (e) The associated SAED pattern.

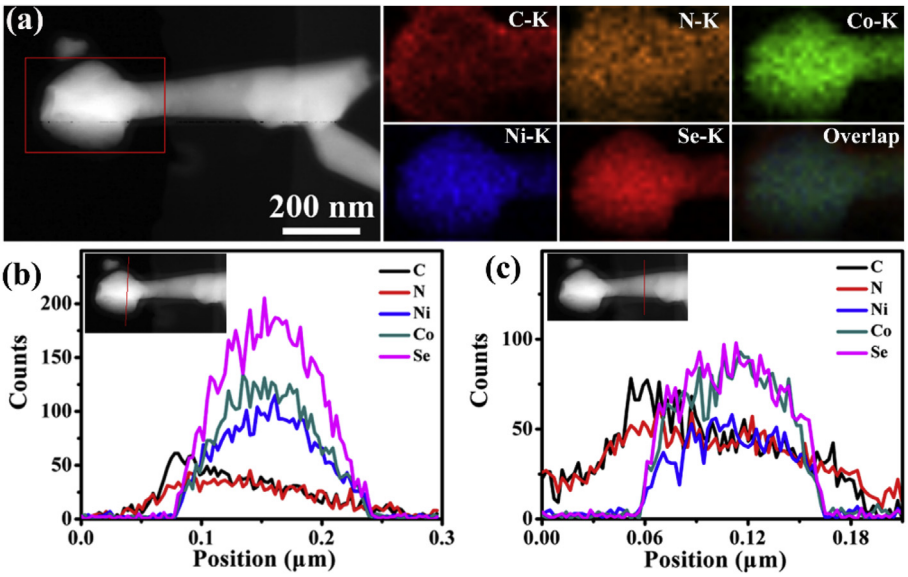

Fig. 5. (a) The element mapping images of $NiCoSe_{2-x}$/NC core/shell nanorod showing the element distribution of C, Ni, Co and Se. (b–c) The line-scan images of the nanoparticles and the nanorod, respectively.

$NiCoSe_{2-x}$/NC core/shell nanorod electrode exhibits a much lower onset potential at 1.48 V. In addition, it only requires a low overpotential of 215 mV to reach a current density of 10 mA/cm^2, which is remarkably lower than that of Ni_3Se_4 (443 mV) and CoSe (338 mV). The $NiCoSe_{2-x}$/NC core/shell nanorod electrode also has the lowest Tafel slope of 75 mV dec^{-1}, lower than 90 mA dec^{-1} of Ni_3Se_4 and 85 mV dec^{-1} of CoSe, indicating the highly promoted kinetics during the OER. The OER performance of the $NiCoSe_{2-x}$/NC core/shell nanorod electrode is better than or comparable to Ni and Co based OER catalysts including NiS [32], CoS [33], $NiCo_2S_4$ [30], $NiSe_2$ [34] and CoSe [35], and those list in Table 2.

Electrochemical impedance spectroscopy (EIS) was performed to investigate the charge transfer kinetics of the catalysts. The Nyquist plots in Fig. 7d can be fitted by the model including the equivalent series resistance (R_s), charge transfer resistance (R_{ct}) and constant phase element related to the electrochemical double capacitance. It is found that the $NiCoSe_{2-x}$/NC core/shell nanorod electrode has the lowest charge transfer resistance of 12 Ω (78 Ω for CoSe and 82 Ω for Ni_3Se_4), demonstrating that fastest charge transfer kinetics in the OER.

Stability is one of the most important parameters of electrocatalysts for practical use. Fig. 7c shows the long-term stability of the $NiCoSe_{2-x}$/NC core/shell nanorod electrode either at fixed potential of 1.57 V by chronoamperometry, or at fixed current density of 100 mA cm^{-2} by chronopotentiometry. It is found that under both case during the catalyst shows good stability over 10 h operation. While both the CoSe and Ni_3Se_4 exhibit interior stability (Fig. S5). We further used SEM, TEM, and XPS to characterize the

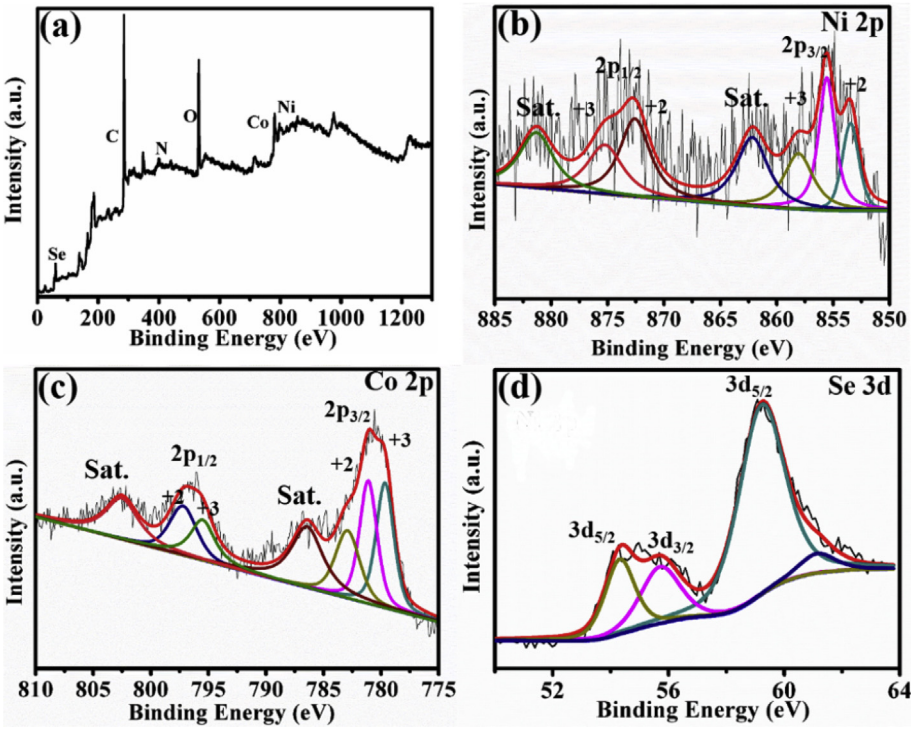

Fig. 6. (a) The XPS survey spectrum of $NiCoSe_{2-x}$/NC. (b–d) The XPS spectra of Ni 2p, Co 2p and Se 3d of $NiCoSe_{2-x}$/NC (Sat. means shake-up satellites).

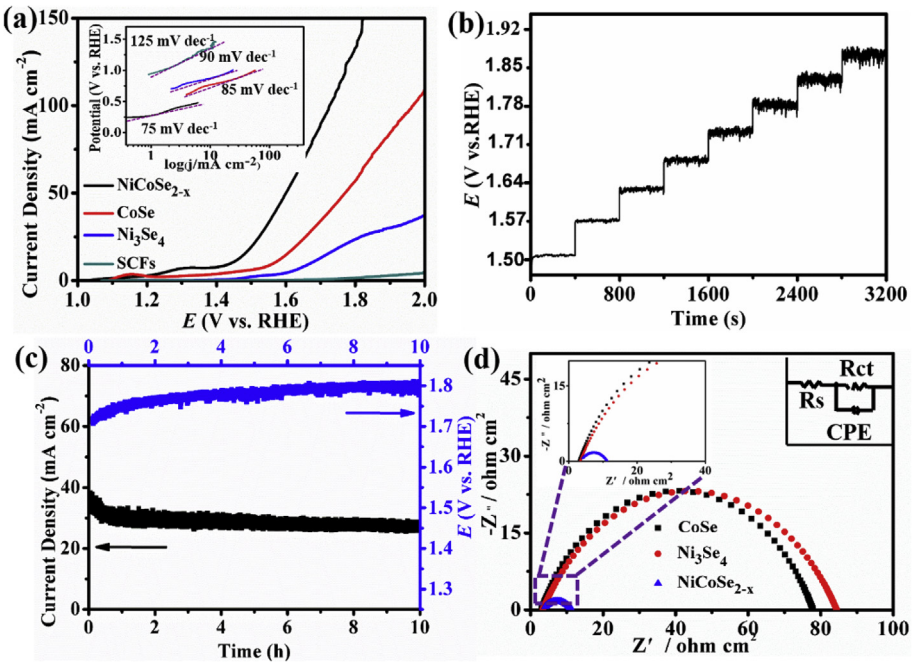

Fig. 7. (a) The polarization curves of $NiCoSe_{2-x}$/NC, Ni_3Se_4, CoSe and silk-derived carbon fibers. The inset image shows corresponded Tafel slop. (b) The multi-step chronopotentiometric curves for the $NiCoSe_{2-x}$/NC. (c) Time-dependent current density and chronopotentiometric curves for the $NiCoSe_{2-x}$/NC. (d) The Nyquist impedance plots curves of $NiCoSe_{2-x}$/NC, Ni_3Se_4 and CoSe, respectively.

tested catalyst. SEM and TEM indicate the mushroom-like morphology of the core/shell nanorod survives after stability test (Fig. S6). The XPS results (Fig. S7) suggest that the surface of the catalyst has been partially oxidized which is common in most metal selenide OER catalysts.

Besides the outstanding OER activity, the HER performance of $NiCoSe_{2-x}$/NC core/shell nanorod electrodes was also characterized in 0.5 M H_2SO_4. The HER polarization curves of all the samples were recorded after 400 CV scans as shown in Fig. 8a. As a control, the HER performance of Pt is also illustrated, which is in good agreement with those in literature [36]. The $NiCoSe_{2-x}$/NC core/shell nanorod electrode shows a low onset potential of −52 mV, much

Table 2
Comparison of the OER activity of the $NiCoSe_{2-x}$/NC nanomushroom arrays with other electrocatalysts.

Catalysts	Electrolyte	Structures	Overpotentials at η_{10} (mV)	Tafel slope (mV·dec^{-1})	Reference
$NiCoSe_{2-x}$/NC	1.0 M KOH	Nanomushroom	215	75	This work
NiS	1.0 M KOH	Nanosheet	212	43	[32]
CoS	1.0 M KOH	Nanosheet	306	72	[33]
$NiCo_2S_4$	1.0 M KOH	Nanowire	260	40.1	[30]
$NiSe_2$	1.0 M KOH	Nanoparticles	295	82	[34]
CoSe	1.0 M KOH	Nanobelts	450	49	[35]

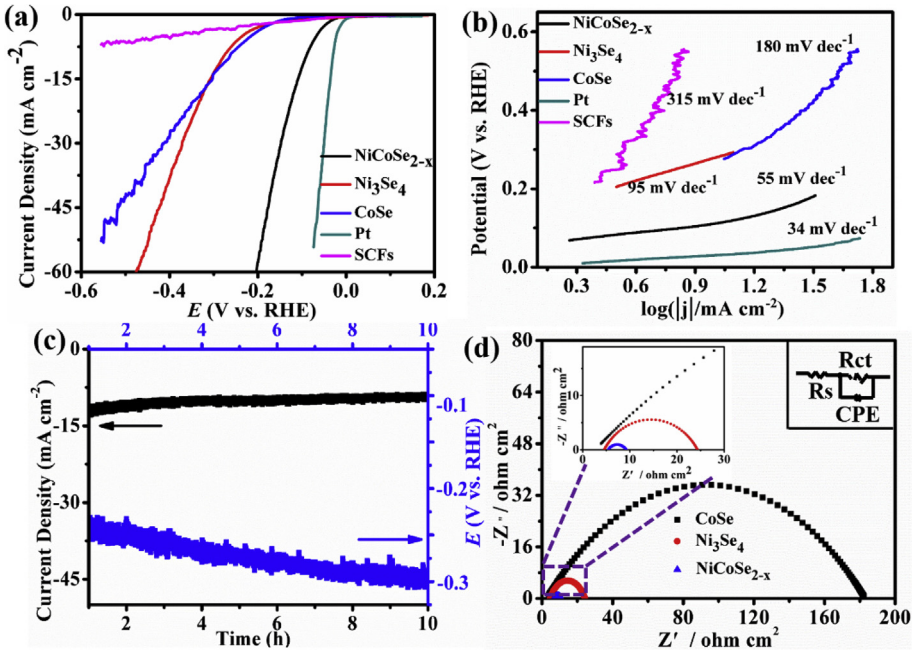

Fig. 8. (a) The polarization curves of $NiCoSe_{2-x}$/NC, Ni_3Se_4, CoSe and silk-derived carbon fibers. (b) The corresponding Tafel slope. (c) Time dependent current density and chronopotentiometric curves for the $NiCoSe_{2-x}$/NC. (d) The Nyquist impedance plots curves of $NiCoSe_{2-x}$/NC, Ni_3Se_4 and CoSe, respectively. All the test condition was in 0.5 M H_2SO_4.

lower than −200 mV of Ni_3Se_4 and -180 mV of CoSe. The overpotential at 10 mA cm^{-2} is 89 mV, 279 mV and 263 mV for the $NiCoSe_{2-x}$/NC, Ni_3Se_4 and CoSe electrodes, respectively (Fig. 8a). The Tafel slope of the $NiCoSe_{2-x}$/NC core/shell nanorod electrode is 55 mV dec^{-1}, which is almost two times lower than that of Ni_3Se_4 (95 mV dec^{-1}), and much lower than that of CoSe (180 mV dec^{-1}) as shown in Fig. 8b. For comparison, we summarized the overpotentials of most recently developed Ni and Co based HER electrocatalysts such as NiS_2 [37], CoS_2 [38], $NiCo_2S_4$ [30], $NiSe_2$ [39], $CoSe_2$ [40] and $Ni_{0.89}Co_{0.11}Se_2$ [22] in Table 3. The $NiCoSe_{2-x}$/NC core/shell nanorod electrode shows comparable HER performance.

The long-term stability of the $NiCoSe_{2-x}$/NC core/shell nanorod electrode in HER was also investigated. The Ni_3Se_4 and CoSe show much lower current density at the same overpotential and poor stability (Fig. S8). While the $NiCoSe_{2-x}$/NC core/shell nanorods electrodes displays good stability, evidenced by the moderate decrease of the current density (Fig. 8c). The profile of the polarization curves before and after the stability test shows a slight shift with the increase of the overpotential at 10 mA cm^{-2} of about 37 mV. And the polarization curve after 5000 cycles and initial one are shown in Fig. S12. We further characterized catalyst after the long-term stability test using SEM, TEM and XPS, as shown in Fig. S9 and Fig. S10. We can conclude that the $NiCoSe_{2-x}$/NC core/shell nanorod electrocatalyst has good stability in both the mushroom-like nanorod structure and the chemical states. The XPS spectra for N1s and the elemental composition after the stability test were also attached in the supporting information as Fig. S13 and Table S1, respectively.

The mechanism of the high HER performance was also explored by EIS. The Nyquist plots in Fig. 8d can also be fitted by a model

Table 3
Comparison of the HER activity of the $NiCoSe_{2-x}$/NC nanomushroom arrays with other electrocatalysts.

Catalysts	Electrolyte	Structures	Overpotentials at η_{10} (mV)	Tafel slope (mV·dec^{-1})	Reference
$NiCoSe_{2-x}$/NC	0.5 M H_2SO_4	Nanomushroom	89	55	This work
NiS_2	0.5 M H_2SO_4	Nanosheet	121	37	[37]
CoS_2	0.5 M H_2SO_4	nanowire	145	51.6	[38]
$NiCo_2S_4$	1 M KOH	Nanowire	210	58.9	[30]
$NiSe_2$	0.5 M H_2SO_4	Nanosheets	135	37.3	[39]
$CoSe_2$	0.5 M H_2SO_4	Nanoparticles	137	40	[40]
$Ni_{0.89}Co_{0.11}Se_2$	0.5 M H_2SO_4	Nanosheet	52	39	[22]

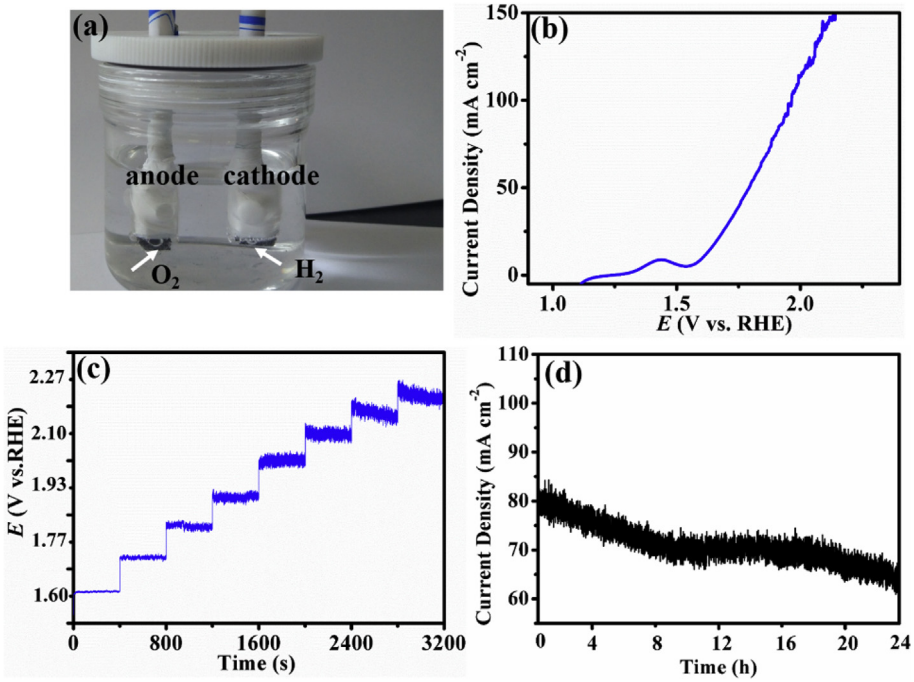

Fig. 9. (a) The optical photograph of the working diagram. (b) The polarization of the $NiCoSe_{2-x}$/NC as anode and cathode for overall water splitting in two-electrode system, respectively. (c) The multi-step chronopotentiometric curves for the $NiCoSe_{2-x}$/NC. (d) Time dependent current density curves for $NiCoSe_{2-x}$/NC with a constant overpotentials of 730 mV. All the test condition was in 1 M KOH.

consisted of R_s, R_{ct} and CPE, similar with the model used for OER. The $NiCoSe_{2-x}$/NC core/shell nanorod electrode has the lowest charge transfer resistance of only 9 Ω, significantly much lower than that of Ni_3Se_4 (~24 Ω) and CoSe (~180 Ω). Furthermore, the $NiCoSe_{2-x}$/NC core/shell nanorod electrode has the largest electrochemically active surface area (ECSA) (Fig. S11). The ECSA of the $NiCoSe_{2-x}$/NC core/shell nanorod 168.3 mF cm^{-2}, almost two times higher than 85.0 mF cm^{-2} of the Ni_3Se_4 and four times higher than 35.7 mF cm^{-2} of CoSe, respectively. The high ECSA indicates more active sites contributed to the HER process.

We further calculated the turnover frequency (TOF) which reflects the intrinsic activity of electrocatalyst [41]. The TOF value of 0.12 s^{-1} for the $NiCoSe_{2-x}$ is two times higher than that of CoSe (0.065 s^{-1}), and four times higher than that of Ni_3Se_4 (0.027 s^{-1}) at overpotential of 300 mV, respectively. The highly promoted charge transfer of the $NiCoSe_{2-x}$/NC core/shell nanorod is probably a synergistic effect of the one-dimensional structure and the N-doped carbon shell, which significantly improves the electrical conductivity. In addition, N-doped carbon materials also shows positive effect in HER. As a result, the present one-dimensional core/shell structure not only facilitate the charge transfer, but also highly increase the number of active sites and intrinsic activity.

Since the high OER and HER activity of the present $NiCoSe_{2-x}$/NC core/shell nanorod, we further employed it as a bifunctional electrocatalyst to drive overall water splitting in 1 M KOH (Fig. 9a). It is found that the cell voltage to reach a current density of 10 mA cm^{-2} is as low as 1.53 V (Fig. 9b). The multi-step chronopotentialmetric measurement indicates the cell can stably drive water splitting to produce hydrogen and oxygen at the cathode and the anode (Fig. 9a), respectively, at selected cell voltages (Fig. 9c). The bifunctional $NiCoSe_{2-x}$/NC core/shell nanorod electrode can stably split water over 24 h with a slight decay of the current density (Fig. 9d).

4. Conclusion

In summary, we reported a novel mushroom-like $NiCoSe_{2-x}$/N-doped C core-shell nanorod arrays on silk-derived carbon fibers *via* a facile one-step selenization. The mushroom-like core/shell nanorod structure was systematically characterized. Thanks to the unique structure, the catalyst shows outstanding OER and HER activity, as well as good long-term stability. It hence efficiently drives the overall water splitting with a low cell voltage of 1.53 V to reach 10 mA cm^{-2}. The high performance is the synergistic effect of the unique one-dimensional core/shell structure which facilitates the charge transfer, and the increased active sites. The carbon shell not only provide a pathway for the electron transfer, but also prevent the internal $NiCoSe_{2-x}$ catalyst from corrosion by the electrolyte. The present work will provide a new vision for preparing the highly efficient electrocatalysts for water splitting.

Acknowledgments

This study was supported by the National Natural Science Foundation of China (NSFC) (Grant number. 51573166), Fundamental Research Funds for the Central Universities (Grant No. JB171401) and Starting Research Fund of Xidian University (Grant No. 10251170002).

Appendix A. Supplementary data

Supplementary data related to this article can be found at https://doi.org/10.1016/j.electacta.2018.04.032.

References

[1] X.X. Zou, Y. Zhang, Noble metal-free hydrogen evolution catalysts for water

splitting, Chem. Soc. Rev. 44 (2015) 5148–5180.
[2] J. Chow, R.J. Kopp, P.R. Portney, Energy resources and global development, Science 302 (2003) 1528–1531.
[3] D.S. Kong, J.J. Cha, H.T. Wang, H.R. Lee, Y. Cui, First-row transition metal dichalcogenide catalysts for hydrogen evolution reaction, Energy Environ. Sci. 6 (2013) 3553–3558.
[4] H.C. Yang, Y.J. Zhang, F. Hu, Q.B. Wang, Urchin-like CoP nanocrystals as hydrogen evolution reaction and oxygen reduction reaction dual-electrocatalyst with superior stability, Nano Lett. 15 (2015) 7616–7620.
[5] H.L. Liu, F. Nosheen, X. Wang, Noble metal alloy complex nanostructures: controllable synthesis and their electrochemical property, Chem. Soc. Rev. 44 (2015) 3056–3078.
[6] Q.C. Dong, Q. Wang, Z.Y. Dai, H.J. Qiu, X.C. Dong, MOF-derived Zn-Doped $CoSe_2$ as an efficient and stable free-standing catalyst for oxygen evolution reaction, ACS Appl. Mater. Interfaces 8 (2016) 26902–26907.
[7] H.Y. Jin, J. Wang, D.F. Su, Z.Z. Wei, Z.F. Pang, Y. Wang, In situ cobalt-cobalt oxide/N-doped carbon hybrids as superior bifunctional electrocatalysts for hydrogen and oxygen evolution, J. Am. Chem. Soc. 137 (2015) 2688–2694.
[8] L. Cheng, W.J. Huang, Q.F. Gong, C.H. Liu, Z. Liu, Y.G. Li, H.J. Dai, Ultrathin WS_2 nanoflakes as a high-performance electrocatalyst for the hydrogen evolution reaction, Angew. Chem. Int. Ed. 53 (2014) 7860–7863.
[9] Q. Gao, C.Q. Huang, Y.M. Ju, M.R. Gao, J.W. Liu, D. An, C.H. Cui, Y.R. Zheng, W.X. Li, S.H. Yu, Phase-selective syntheses of cobalt telluride nanofleeces for efficient oxygen evolution catalysts, Angew. Chem. Int. Ed. 56 (2017) 7877–7881.
[10] J.F. Xie, J.J. Zhang, S. Li, F. Grote, X.D. Zhang, H.R. Wang, X.Y. Lei, B.C. Pan, Y. Xie, Controllable disorder engineering in oxygen-incorporated MoS_2 ultrathin nanosheets for efficient hydrogen evolution, J. Am. Chem. Soc. 135 (2013) 17881–17888.
[11] J. Yang, H.S. Shin, Recent advances in layered transition metal dichalcogenides for hydrogen evolution reaction, J. Mater. Chem. A 2 (2014) 5979–5985.
[12] B.M. Hunter, H.B. Gray, A.M. Müller, Earth-abundant heterogeneous water oxidation catalysts, Chem. Rev. 116 (2016) 14120–14136.
[13] Z.H. Xia, L. An, P. Chen, D.J. Xia, Non-Pt nanostructured catalysts for oxygen reduction reaction: synthesis, catalytic activity and its key factors, Adv. Energy Mater. 6 (2016) 1600458.
[14] Y.W. Liu, H. Cheng, M.J. Lyu, S.J. Fan, Q.H. Liu, W.S. Zhang, Y.D. Zhi, C.M. Wang, C. Xiao, S.Q. Wei, B.J. Ye, Y. Xie, Low overpotential in vacancy-rich ultrathin $CoSe_2$ nanosheets for water oxidation, J. Am. Chem. Soc. 136 (2014) 15670–15675.
[15] M. Chhowalla, H.S. Shin, G. Eda, L.J. Li, K.P. Loh, H. Zhang, The chemistry of two-dimensional layered transition metal dichalcogenide nanosheets, Nat. Chem. 5 (2013) 263–275.
[16] R. Wu, J.F. Zhang, Y.M. Shi, D.L. Liu, B. Zhang, Metallic WO_2-carbon mesoporous nanowires as highly efficient electrocatalysts for hydrogen evolution reaction, J. Am. Chem. Soc. 137 (2015) 6983–6986.
[17] H.F. Liang, A.N. Gandi, D.H. Anjum, X.B. Wang, U. Schwingenschlögl, H.N. Alshareef, Plasma-assisted synthesis of NiCoP for efficient overall water splitting, Nano Lett. 16 (2016) 7718–7725.
[18] W. Li, X.F. Gao, X.G. Wang, D. Xiong, P.P. Huang, W.G. Song, X. Bao, L.F. Liu, From water reduction to oxidation: janus Co-Ni-P nanowires as high-efficiency and ultrastable electrocatalysts for over 3000 h water splitting, J Power Sources 330 (2016) 156–166.
[19] J.F. Chang, Y. Xiao, M.L. Xiao, J.J. Ge, C.P. Liu, W. Xing, Surface oxidized cobalt-phosphide nanorods as an advanced oxygen evolution catalyst in alkaline solution, ACS Catal. 5 (2015) 6874–6878.
[20] X. Xu, F. Song, X.L. Hu, A nickel iron diselenide-derived efficient oxygen-evolution catalyst, Nat. Commun. 7 (2016) 12324.
[21] H.X. Zhang, Q. Ding, D.H. He, H. Liu, W. Liu, Z.J. Li, B. Yang, X.W. Zhang, L.C. Lei, S. Jin, A p-Si/$NiCoSe_x$ core/shell nanopillar array photocathode for enhanced photoelectrochemical hydrogen production, Energy Environ. Sci. 9 (2016) 3113–3119.
[22] B. Liu, Y.F. Zhao, H.Q. Peng, Z.Y. Zhang, C.K. Sit, M.F. Yuen, T.R. Zhang, C.S. Lee, W.J. Zhang, Nickel-cobalt diselenide 3D mesoporous nanosheet networks supported on Ni foam: an all-pH highly efficient integrated electrocatalyst for hydrogen evolution, Adv. Mater. (2017) 1606521.
[23] W.J. Zhou, J. Jia, J. Lu, L.J. Yang, D.M. Hou, G.Q. Li, S.W. Chen, Recent developments of carbon-based electrocatalysts for hydrogen evolution reaction, Nano Energy 28 (2016) 29–43.
[24] M.R. Gao, X. Cao, Q. Gao, Y.F. Xu, Y.R. Zheng, J. Jiang, S.H. Yu, Nitrogen-doped graphene supported $CoSe_2$ nanobelt composite catalyst for efficient water oxidation, ACS Nano 8 (2014) 3970–3978.
[25] X.W. Xu, Y.C. Ge, M. Wang, Z.Q. Zhang, P. Dong, R. Baines, M.X. Ye, J.F. Shen, Cobalt-doped $FeSe_2$-RGO as highly active and stable electrocatalysts for hydrogen evolution reactions, ACS Appl. Mater. Interfaces 8 (2016) 18036–18042.
[26] Q. Liu, J.T. Jin, J.Y. Zhang, $NiCo_2S_4$@graphene as a bifunctional electrocatalyst for oxygen reduction and evolution reactions, ACS Appl. Mater. Interfaces 5 (2013) 5002–5008.
[27] S.Y. Wang, L.P. Zhang, Z.H. Xia, A. Roy, D.W. Chang, J.B. Baek, L.M. Dai, BCN graphene as efficient metal-free electrocatalyst for the oxygen reduction reaction, Angew. Chem. Int. Ed. 51 (2012) 4209–4212.
[28] X. Li, L. Zhang, M.R. Huang, S.Y. Wang, X.M. Lie, H.W. Zhu, Cobalt and nickel selenide nanowalls anchored on graphene as bifunctional electrocatalysts for overall water splitting, J. Mater. Chem. A 4 (2016) 14789–14795.
[29] B. Yang, L. Yu, H.J. Yan, Y.B. Sun, Q. Liu, J.Y. Liu, D.L. Song, S.X. Hu, Y. Yuan, L.H. Liu, J. Wang, Fabrication of urchin-like $NiCo_2(CO_3)_{1.5}(OH)_3$@$NiCo_2S_4$ on Ni foam by an ion-exchange route and application to asymmetrical supercapacitors, J. Mater. Chem. A 3 (2015) 13308–13316.
[30] A. Sivanantham, P. Ganesan, S. Shanmugam, Hierarchical $NiCo_2S_4$ nanowire arrays supported on Ni foam: an efficient and durable bifunctional electrocatalyst for oxygen and hydrogen evolution reactions, Adv. Funct. Mater. 26 (2016) 4661–4672.
[31] C.C. Sun, Q.C. Dong, J. Yang, Z.Y. Dai, J.J. Lin, P. Chen, W. Huang, X.C. Dong, Metal–organic framework derived $CoSe_2$ nanoparticles anchored on carbon fibers as bifunctional electrocatalysts for efficient overall water splitting, Nano Research 9 (2016) 2234–2243.
[32] J.S. Chen, J.W. Ren, M. Shalom, T. Fellinger, M. Antonietti, Stainless steel mesh-supported NiS nanosheet array as highly efficient catalyst for oxygen evolution reaction, ACS Appl. Mater. Interfaces 8 (2016) 5509–5516.
[33] J. Wang, H.X. Zhong, Z.L. Wang, F.L. Meng, X.B. Zhang, Integrated three-dimensional carbon paper/carbon tubes/cobalt-sulfide sheets as an efficient electrode for overall water splitting, ACS Nano 10 (2016) 2342–2348.
[34] Z.H. Pu, Y.L. Luo, A.M. Asiri, X.P. Sun, Efficient electrochemical water splitting catalyzed by electrodeposited nickel diselenide nanoparticles based film, ACS Appl. Mater. Interfaces 8 (2016) 4718–4723.
[35] M.R. Gao, Y.F. Xu, J. Jiang, Y.R. Zheng, S.H. Yu, Water oxidation electrocatalyzed by an efficient Mn_3O_4/$CoSe_2$ nanocomposite, J. Am. Chem. Soc. 134 (2012) 2930–2933.
[36] Y.G. Li, H.L. Wang, L.M. Xie, Y.Y. Liang, G.S. Hong, H.J. Dai, MoS_2 nanoparticles grown on graphene: an advanced catalyst for the hydrogen evolution reaction, J. Am. Chem. Soc. 133 (2011) 7296–7299.
[37] J.Q. Yan, H. Wu, P. Li, H. Chen, R.P. Jiang, S.Z. Liu, $Fe_{(III)}$ doped NiS_2 nanosheet: a highly efficient and low-cost hydrogen evolution catalyst, J. Mater. Chem. A 5 (2017) 10173–10181.
[38] M.S. Faber, R. Dziedzic, M.A. Lukowski, N.S. Kaiser, Q. Ding, S. Jin, High-performance electrocatalysis using metallic cobalt pyrite (CoS_2) micro- and nanostructures, J. Am. Chem. Soc. 136 (2014) 10053–10061.
[39] H.F. Liang, L.S. Li, F. Meng, L.N. Dang, J.Q. Zhuo, A. Forticaux, Z.C. Wang, S. Jin, Porous two-dimensional nanosheets converted from layered double hydroxides and their applications in electrocatalytic water splitting, Chem. Mater. 27 (2015) 5702–5711.
[40] D.S. Kong, H.T. Wang, Z.Y. Lu, Y. Cui, $CoSe_2$ nanoparticles grown on carbon fiber paper: an efficient and stable electrocatalyst for hydrogen evolution reaction, J. Am. Chem. Soc. 136 (2014) 4897–4900.
[41] H.Q. Zhou, F. Yu, Y.F. Huang, J.Y. Sun, Z. Zhu, R.J. Nielsen, R. He, J.M. Bao, W.A. Goddard, S. Chen, Z.F. Ren, Efficient hydrogen evolution by ternary molybdenum sulfoselenide particles on self-standing porous nickel diselenide foam, Nat. Commun. 7 (2016) 12765.